Lagrangian description of the unsteady flow induced by a single pulse of a jellyfish

Jin-Tae Kim[1] and Leonardo P. Chamorro[1,2,3,*]

[1]*Mechanical Science and Engineering Department, University of Illinois, Urbana, Illinois 61801, USA*
[2]*Civil and Environmental Engineering Department, University of Illinois, Urbana, Illinois 61801, USA*
[3]*Aerospace Engineering Department, University of Illinois, Urbana, Illinois 61801, USA*

(Received 11 December 2018; published 6 June 2019)

Lagrangian statistics and pair dispersion induced by an isolated pulse of a small jellyfish, *Aurelia aurita*, were quantified and characterized using 3D particle tracking velocimetry (3D-PTV). Probability density functions (PDF) of the Lagrangian velocity components indicated more intense mixing in the radial direction and revealed three stages dominated by flow acceleration, mixing, and dissipation. Time evolution of the Lagrangian acceleration variance further illustrates each phase. During the mixing phase, the flow shares characteristics of homogeneous isotropic turbulence. In addition, we show that a single pulse may induce rich wake dynamics characterized by pair dispersion with a super-diffusive t^3 regime due to large-scale flow inhomogeneity, followed by a coherent t^2-Batchelor scaling and then t^1-Brownian motions. The first trend occurred in the accelerated flow, whereas the second dynamic was observed in the mixed wake and depended on the initial separation. The Brownian motion was present in the late stage dominated by flow dissipation. Kolmogorov microscales during the fully mixed phase were obtained with three distinct approaches, namely, Heisenberg-Yaglom relation of the Lagrangian acceleration variance, the fluctuating rate of the strain tensor in the Eulerian frame of reference as well as the Batchelor scaling in pair dispersion, which showed good agreement.

DOI: 10.1103/PhysRevFluids.4.064605

I. INTRODUCTION

Lagrangian dynamics has provided significant insight on mixing and transport, especially in the case of fully developed turbulence [1–4]. These processes can be described in terms of the pair dispersion $R^2(t)$, which refers to the temporal evolution of the distance between two fluid particles. Richardson [5] and Obukhov [6] proposed a dispersion law $R^2(t) = g\langle\epsilon\rangle t^3$ in the inertial subrange $t \ll T_L$, where g is a constant, $\langle\epsilon\rangle$ is the mean energy dissipation rate per unit of mass, and T_L is the integral correlation timescale. Later, Batchelor [7] suggested that the initial separation of the fluid particles $\mathbf{r}_0$ plays a role in the dispersion and proposed $R^2(t) \propto (\langle\epsilon\rangle\|\mathbf{r}_0\|)^{2/3}t^2$ in the inertial subrange $t < t_0$, where t_0 is a characteristic timescale related to $\mathbf{r}_0$ [8]. The Richardson-Obukhov typically holds for $t_0 < t < T_L$, whereas fluid particles disperse following $R^2(t) \propto t$ at long times $t \gg T_L$ as the turbulence is expected to be diffusive.

Substantial effort on pair dispersion has been placed on isotropic turbulence [9]. Bourgoin *et al.* [8] measured relative dispersion under high-turbulence levels using an optical particle tracking approach. They found that $\mathbf{r}_0$ plays an important role, as predicted by Batchelor, in almost all turbulent flows. In addition, they pointed out that a fully developed Richardson-Obukhov scaling

*lpchamo@illinois.edu

regime, $R^2(t) \propto t^3$, requires a large separation between T_L and t_0, such that the turbulence level should be higher than the one occurring in most practical situations. Sawford *et al.* [10] numerically investigated pair dispersion on scenarios similar to experiments by Bourgoin *et al.* [8] and Ouellette *et al.* [11]. Their results were comparable to earlier DNS [4,12,13] and improved collapse of data when compensated by the inertial subrange scaling laws that depend on $\langle \epsilon^{1/3} \rangle$. Recent efforts have gone toward characterizing pair dispersion in anisotropic and environmental flows, such as the convective turbulence in Rayleigh-Bénard cells [14,15] and ocean current at the surface of the Gulf of Mexico [16]. Very recently, Polanco *et al.* [17] investigated numerically the pair dispersion in a turbulent channel flow. They found that strong flow inhomogeneity can induce a super-diffusive regime similar to the t^3 Richardson-Obukhov scaling due to large-scale shear.

Another remarkable feature of turbulent mixing involves relatively strong Lagrangian acceleration. Various studies have focused on high-acceleration events in isotropic turbulence [18]. La Porta *et al.* [1] observed acceleration in excess of 1 500 times the gravity and found that probability density function of the Lagrangian acceleration has stretched exponential shape. Biferale *et al.* [4] and Toschi *et al.* [19] noted that fluid particles can stay in a small-scale vortex for a time exceeding the local eddy turnover time. Material acceleration has been found to be highly intermittent; intense fluctuations can be associated to small-scale vortical structures [2,3]. Few studies have investigated Lagrangian acceleration in anisotropic and inhomogenous turbulent flows including convective turbulence [15,20,21], jet flows [22], channel [23], and porous-media flows [24].

Associated investigations of Lagrangian mixing, pair dispersion, and transport properties in unsteady flows, e.g., those induced by marine organisms is very limited. Here, we explored a particular case of the impact of a single pulse from a jellyfish. No attempt is made to link our findings to marine mixing or elaborate on biology-related implications. We just show the rich dynamics induced by a single pulse of this swimmer, which uses bell contraction and relaxation (CR) through jetting and paddling [25–27]. These mechanisms produce vortex rings and fluid ejection from the inner cavity of the bell [28–31], which trigger rich fluid dynamics.

We used 3D particle tracking velocimetry [32–34] to uncover, for the first time, distinctive Lagrangian dynamics. The work provides new quantitative information on Lagrangian statistics, such as acceleration, and pair dispersion. It is worth pointing out that the analysis uses concepts from homogeneous isotropic turbulence (HIT) [2,18]. We focused on a specific instance, where a jellyfish placed in a quiescent medium underwent a sufficiently long inactive phase after a pulse to isolate the effect of a single CR process (see basic inspection in Fig. 1).

II. EXPERIMENTAL SETUP AND APPROACH

A. Laboratory setup

Flow measurements were performed with 3D particle tracking velocimetry, which was optimized to capture the acceleration and trajectory of the induced flow over a swimming cycle. The jellyfish (*Aurelia aurita*) was obtained from Jellyfish Art and maintained in 20-L aquaria circular tank at 22 °C. The water quality parameters including salinity, pH level, Ammonia, Nitrite and Nitrate, were carefully monitored and preserved for the health of the jellyfish prior to testing. The swimmer had maximum bell diameter of $d = 35$ mm with a fineness ratio of $f = 0.23$. Here, the fineness ratio is below the critical one $f_c = 0.265$, where paddling appears to play a key role on the thrust generation [26].

The jellyfish was gently placed in quiescent water contained in a transparent, cubic tank of side $\sim 9d$. Wall effects are considered negligible as the focus is placed on the near wake. The medium was seeded with 55 μm silver-coated glass spheres with the density of 1.1 g/cm^3. The salinity of the fluid in each tank was kept at a specific gravity of 1.022 and water temperature was constant to minimize the likelihood of irregular motion. The specimen was moved in the tank only during the experiments to minimize the effects of tank geometry and seeding particles [Fig. 1(a)]. This was achieved using an acrylic tube of $\sim 1.1d \times \sim 1.1d$ cross section and $\sim 3d$ long whose end was

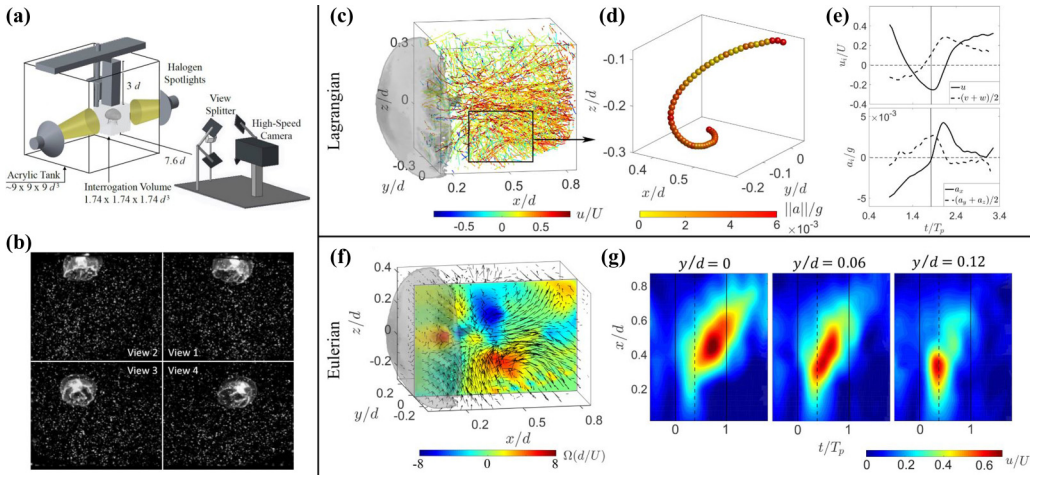

FIG. 1. Jellyfish wake in Lagrangian and Eulerian frames of reference. (a) Basic setup. (b) four-image stereo view. (c) Sample flow trajectories; colors denote axial velocity u normalized by the maximum body velocity $U = 28$ mm s^{-1}. (d) Single-particle trajectory in the vicinity of the bell margin; the color represents acceleration magnitude $\|a\|/g$, every 20 instants. (e) Velocity and acceleration of the trajectory from Fig. 1(d) in the axial and radial directions. (f) 3D Eulerian instantaneous velocity field with in-plane vorticity field, indicating the presence of a vortex ring. (g) Axial velocity field along x for various radial locations as a function of time; the solid and dotted lines indicate instants at maximum and minimum bell diameters.

located $3d$ below the free surface but above the interrogation volume. It ensured the jellyfish to move down through the interrogation volume with minimum external disturbance.

We measured multiple swimming cycles and selected that with a significantly long inactive phase $t_{\text{inactve}} = 2.4T_p$, where T_p is the interval needed to perform the CR. This allows to investigate the immediate effect of the jellyfish pulse, because multiple swimming cycles may affect pair dispersion dynamics in spatial-temporal domain. Henceforth the time $t = 0$ defines the beginning of the contraction phase.

B. 3D particle tracking velocimetry

Images were recorded with a Mikrotron EoSens 4CXP MC4082 high-speed camera at 550 fps and 4 MP. A Nikon AF Micro-Nikkor 60 mm with a focal ratio f/2.8D lens was used to maximize the focus on the investigation volume of 40 mm side. Stereoscopic four-image pairs were obtained with a four-view splitter [35] [Fig. 1(b)] and processed using OpenPTV (http://www.openptv.net). The particles were illuminated by two Stanley Lithium Ion Halogen Spotlights only during the measurement (less than 5 s) to avoid excess heat of the tank and alter the animal's behavior. Effects of camera angles, focal length, distortion coefficients, and refractive index changes along the camera view, i.e., air-acrylic-water [34], were accounted for, which resulted in a calibration error with standard deviation of $\sim 3 \times 10^{-3} d$. To allow better examination of the particle trajectories, the images were masked to show only the relevant regions of interest. The areas containing the initial vortex ring expelled by a single pulse were left unmasked. Based on 2D-PIV measurements [36], the first vortex ring was calculated to extend backwards from the jellyfish in a cone segment with base diameter $\sim 2d$ and height $\sim 1.5d$. It was crucial to obtain long trajectories to properly estimate Lagrangian acceleration. Approximately 4.0×10^5 reconstructed particles were tracked using the so-called Hungarian algorithm, and linked by performing a ten-frame gap closing for longer trajectories. Those trajectories and associated temporal derivatives were evaluated and filtered using

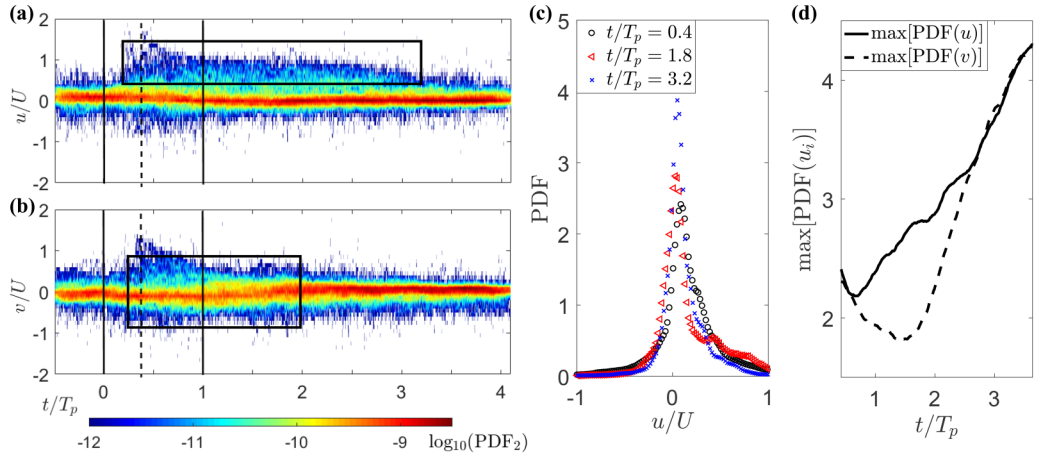

FIG. 2. Lagrangian statistics. The bivariate PDFs of Lagrangian velocity and temporal evolution of the jellyfish propulsion: (a) axial and (b) radial components. (c) Axial velocity PDFs at instants of acceleration ($t/T_p = 0.4$), fully mixed ($t/T_p = 1.8$), and dissipation ($t/T_p = 3.2$) stages. (d) Temporal evolution of the peak of velocity PDFs in the axial and radial directions.

fourth-order B-splines [37]; this approximation resulted the best interpolation scheme for particle tracking in turbulence [38]. Additional details can be found in Refs. [15,22,39].

An inferred 3D Eulerian velocity vector field [Figs. 1(f) and 1(g)] was also obtained by interpolating scattered Lagrangian flow particles at each frame based on the natural neighbor interpolation method. A pair of strong vortex rings was present at $x/d = 0.4$. The jellyfish diameter decreased to near 40% of its maximum during the relaxation phase, indicating that the radial location of the vortex ring occurred near the bell margin location similar to previous results [36,40]. The maximum velocity along the jellyfish axis was during the relaxation phase at $x/d = 0.45$ from the initial position of the jellyfish [Fig. 1(g), left]. Away from the jellyfish center axis in the radial direction, the relative maximum velocity occurred earlier and closer to the jellyfish in streamwise direction [Fig. 1(g), right]. The result indicated that the vortical structure generated by the paddling propagated to the center and combined with the flow induced by the jetting mechanism. It resulted in a wake with relatively high axial velocity lasting significantly long.

III. RESULTS AND DISCUSSION

A. Lagrangian PDFs

Bulk evaluation of the wake showed that entrainment occurred past the contraction, where vortex ring contributed to the radial acceleration, a_r. This acceleration component reached the maximum with the axial counterpart a_x approaching to zero at $t/T_p \approx 1.8$. The conversion of a_r in a_x [Fig. 1(e)] indicates the efficient propulsion mechanism of the jellyfish swimming. The flow underwent acceleration around $t/T_p \approx 0.4$, full development at $t/T_p \approx 1.8$ and dissipation starting at $t/T_p \approx 3.2$ [Fig. 2(a)]. The bivariate PDF of the radial velocity exhibited a wider distribution and lower peaks [within the black box in Fig. 2(b)] compared to the axial velocity [within the black box in Fig. 2(a)]. The Lagrangian velocity distributions of the axial and radial components indicated that the mixing process lasts significantly longer than the duration of the CR with the axial PDF having a low peak with positive skewness that reflect the jetlike effect [Fig. 2(c)]. Right after CR, the velocity PDF peak of the axial component quickly increased, whereas the radial component decreased until $t/T_p \approx 1.8$ [Fig. 2(d)]. The jellyfish induced significant mixing radially and a long-lasting wake over $3T_p$. The acceleration PDF at the acceleration ($t/T_p = 0.4$) and dissipation ($t/T_p = 3.2$) stages (Fig. 3) exhibited heavy tails, indicating the strong intermittency of the Lagrangian motions as in

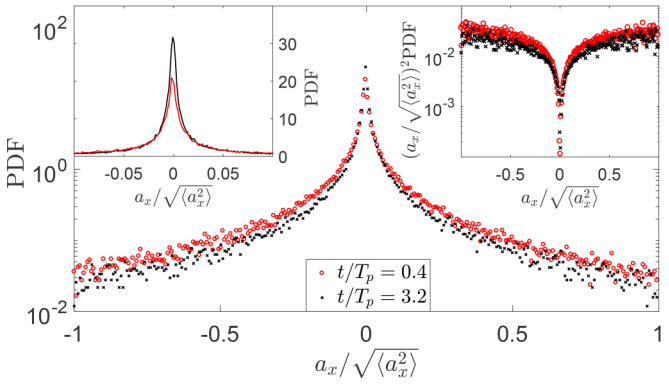

FIG. 3. Lagrangian acceleration statistics. PDF of axial Lagrangian acceleration a_x at instants of acceleration ($t/T_p = 0.4$) and dissipation ($t/T_p = 3.2$) stages. (Inset at right shows the second-order PDF)

isotropic turbulence [4]. During flow acceleration, the PDF exhibited a heavier tails, ∼33% lower peak at zero value (Fig. 3 inset, left) and ∼50% higher in the acceleration variance $\langle a_x^2\rangle$ than the dissipation stage. It is worth pointing out that due to limited number of fluid particles at each phase, the acceleration PDF was resolved up to ±1 root-mean square (rms).

B. Acceleration variance

The variance of flow particle accelerations obtained by Heisenberg and Yaglom [41,42] is given by

$$\langle a_i a_j\rangle = a_0 \epsilon^{3/2} \upsilon^{-1/2} \delta_{ij}, \tag{1}$$

where a_0 is a constant; here we assume $a_0 = 5$. In the case of HIT, $a_0 \approx 3$–5 at $\mathrm{Re}_\lambda \approx 140$ [2]. Note that the value a_0 may be affected by the position uncertainty, filtering method as well as inhomogeneous and anisotropic nature of the flow. The temporal evolution of acceleration variance (Fig. 4) further shows distinctive phases of the jellyfish propulsion which corresponds to the previous analysis on the velocity PDF [Fig. 2(c)]. During the acceleration phase $\Delta t_\mathrm{A} = [0, 0.8]t/T_P$,

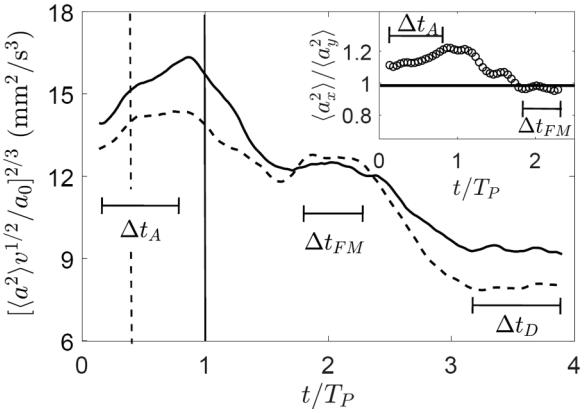

FIG. 4. Variance of the axial (solid curve) and radial (dotted curve) compensated accelerations $[\langle a^2\rangle \upsilon^{1/2}/a_0]^{2/3}$ based on the Heisenberg-Yaglom relation [41,42]. Δt_A, Δt_FM, and Δt_D indicate the intervals of the acceleration, fully mixed, and dissipation phases. The vertical solid and dotted lines indicate instants at maximum and minimum bell diameters. Inset shows the ratio of axial and radial acceleration variances.

the streamwise and radial components increase as well as the ratio $\langle a_x^2\rangle/\langle a_y^2\rangle$ (Fig. 4 inset), reaching upto 1.25; the flow exhibits an increase in anisotropy and Re. In the fully mixed phase $\Delta t_{\rm FM} = [1.7, 2.3]t/T_P$, the variance of both acceleration components show a nearly constant value $[\langle a^2\rangle v^{1/2}/a_0]^{2/3} = \langle \epsilon_v\rangle \approx 12.5\,\mathrm{mm^2\,s^{-3}}$, with $\langle a_x^2\rangle/\langle a_y^2\rangle \approx 1$, similar to isotropic turbulence. At the dissipation phase $\Delta t_{\rm D} > 3t/T_p$, both variance components quickly drop.

C. On the Eulerian quantities

The Lagrangian acceleration variance reveals certain characteristics of HIT during $\Delta t_{\rm FM}$; this suggests that turbulentlike features can be inferred in the Eulerian frame of reference. By decomposing the velocity field u_i during $\Delta t_{\rm FM}$ into the mean $\langle u_i\rangle$ and fluctuating u_i' components, the rms of the velocity fluctuations resulted $\tilde{u} = [(u_x'^2 + u_y'^2 + u_z'^2)/3]^{1/2} \approx 0.007\ \mathrm{m\,s^{-1}}$ with mean velocity $\langle u\rangle = (\langle u_x\rangle + \langle u_y\rangle + \langle u_z\rangle)/3 < 0.2\tilde{u}$, i.e., much smaller than $\tilde{u}$. Further, the jellyfish's Kolmogorov microscale can also be obtained from the fluctuating rate of strain tensor as follows:

$$\langle \epsilon_e\rangle = 2v\langle s_{ij}s_{ij}\rangle,$$
$$\text{where } s_{ij} = \frac{1}{2}\frac{\partial u_i'}{\partial x_j}\frac{\partial u_j'}{\partial x_i}. \tag{2}$$

It contains nine components of the fluctuating velocity gradients. The radial average within d during $\Delta t_{\rm FM}$ results $\langle \epsilon_e\rangle \approx 11.39 \pm 2.3\ \mathrm{mm^2\,s^{-3}}$, which is relatively close to $\langle \epsilon_v\rangle$. The corresponding integral scale and turbulent Reynolds number are $L = \tilde{u}^3/\langle \epsilon_e\rangle \approx 28$ mm and $\mathrm{Re}_\lambda = (15\tilde{u}L/v)^{1/2} \approx 60$. Higher-order turbulence quantities in the Eulerian frame may be not resolved due to the data interpreted from Lagrangian flow trajectories.

D. Pair dispersion

The pair dispersion $R^2(t^*) = \langle \|\mathbf{r}(t^*) - \mathbf{r}_0\|^2\rangle$ is highly influenced by the initial instant and separation due to the transient, anisotropic and nonhomogeneous flow. Indeed, R^2 would reveal distinctively different physics of pair particles for a given $\mathbf{r}_0$ if both are around the margin or located in the margin and center. Consequently, a close look is needed to uncover the underlying dynamics. Here, we considered particle pairs in which one of them always is initially located at the jellyfish center axis $\mathbf{r}_0 = \mathbf{P}_1(x, y, z, t^* = 0) - \mathbf{P}_2(x, y = 0, z = 0, t^* = 0)$ and the other is in a given radial direction. A small initial separation indicates R^2 mostly affected by jetlike flow; whereas large initial separation accounts for the effect of jetting and paddling. We illustrate cases (i) within the minimum jellyfish diameter $\|\mathbf{r}_0\|/d = 0.1$, (ii) in the intermediate distance $\|\mathbf{r}_0\|/d = 0.3$, and (iii) near the maximum jellyfish diameter $\|\mathbf{r}_0\|/d = 0.5$. We also illustrate R^2 at three distinctive instants; namely, those dominated by acceleration ($t/T_p = 0.4$), fully mixed ($t/T_p = 1.8$), and dissipation ($t/T_p = 3.2$) stages.

The R^2 first exhibited a t^2-Batchelor dispersion at $t/T_p = 0.4$ [Fig. 5(a)]. Remarkably, high-rate particle dispersion rate of t^3 occurred at $\|\mathbf{r}_0\|/d = 0.5$. It is worth noting that the t^3 dispersion rate occurs in the case of HIT at very high turbulence [8], known as the Richardson-Obukhov regime. Here, the process leading to such dispersion rate is different, and occurred in a low Reynolds number and turbulence level. This was possibly due to the large-scale inhomogeneity and unsteadiness of the flow during the acceleration phase induced by two propulsive mechanisms, jetting and paddling, which produced mutual flow interaction. Similar result was reported recently in the case of channel flow in Polanco *et al.* [17].

The t^2-Batchelor regime occurred during the mixing regime, similar to HIT [Fig. 5(b)]. In the dissipation phase, R^2 approached to a linear trend as the residual flow exhibited Brownian behavior [Fig. 5(c)].

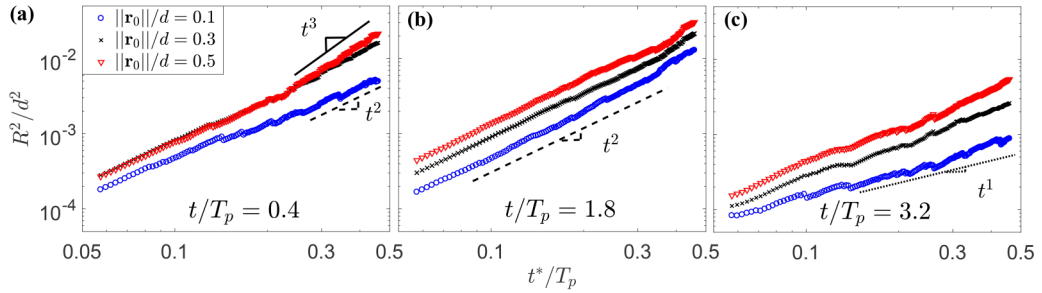

FIG. 5. Pair dispersion. The wake induced by the jellyfish showed rich Lagrangian dynamics exhibiting (a) t^3-Richardson scaling at $t/T_p = 0.4$, (b) coherent t^2-Batchelor scaling as a function of $\|\mathbf{r}(0)\|$ at $t/T_p = 1.8$, and (c) t^1-Brownian motion.

E. Kolmogorov microscales

Batchelor's prediction of $R^2(t^*)$ as a function of $\|\mathbf{r}_0\|$ in the inertial range $t^* < t_0$ is given as follows [7]:

$$R^2(t^*) = S_2 t^{*2},$$
$$\text{for } t^* < t_0 = \left(\frac{\|\mathbf{r}_0\|^2}{\langle\epsilon\rangle}\right)^{1/3}, \tag{3}$$

where $S_2 = \frac{11}{3}C(\langle\epsilon\rangle\|\mathbf{r}_0\|)^{2/3}$ is the second-order structure function in the inertial range of HIT and $C = 2.13$ is an universal constant [8]. The mean energy dissipation rate in the mixing phase is directly obtained, by backsolving using known variables R^2 and $\|\mathbf{r}_0\|$, as $\langle\epsilon\rangle = 11.25 \pm 1.5\ \text{mm}^2\ \text{s}^{-3}$. The associated Kolmogorov microscales resulted $\eta = (\nu^3/\epsilon)^{1/4} \approx 0.5$ mm and $\tau = (\nu/\eta)^{1/2} \approx$

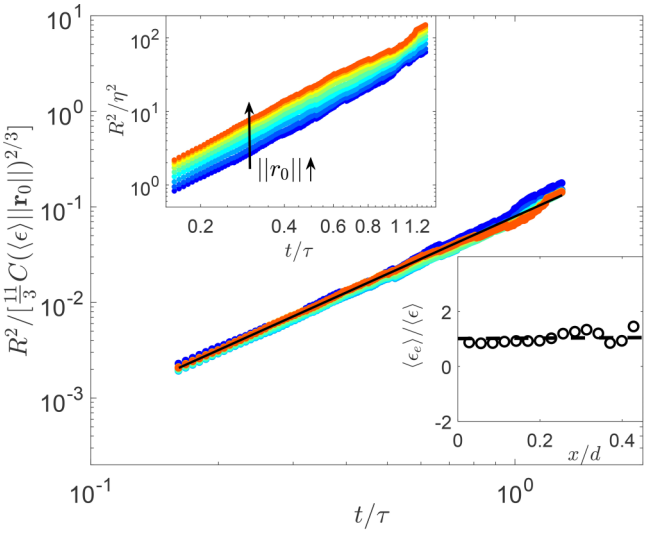

FIG. 6. Normalized pair dispersion R^2 in the mixed phase Δt_{FM}. It includes nine initial separations ranging from $\|\mathbf{r}\|/d = 0.1$ to 0.5 every $\|\Delta\mathbf{r}\|/d = 0.05$. The data and Batchelor's prediction [7] collapse onto a universal power law. The top inset shows the same curves scaled by the Kolmogorov length η. The bottom inset shows the energy dissipation rate computed using Eulerian-based $\langle\epsilon_e\rangle$ and Lagrangian-based $\langle\epsilon\rangle$. The notable match suggests the accurate estimate of the Kolmogorov microscales.

0.28 s. The minimum characteristic timescale resulted $\min\{t_0\}/T_p = 1.3$ at $\|\mathbf{r}_0\|/d = 0.1$, which was larger than the range $t^*/T_P = [0.06, 0.5]$ and satisfied the condition of the Batchelor scaling in the inertial range. Normalization of the R^2 at the various $\mathbf{r}_0$ during the fully mixed phase Δt_{FM} revealed a notable collapse onto a single universal power law that also matched with Batchelor's prediction (Fig. 6). The Kolmogorov microscales obtained from the pair dispersion, the acceleration variance (Fig. 4) and the Eulerian frame of reference agreed reasonably well. The results indicate that the transient wake induced the jellyfish propulsion underwent fully developed stage, which exhibited features of (weak) HIT. Note that η is comparable to the ocean counterpart $\eta_0 = 0.29$–0.52 mm (equivalent to 10^{-5} to 10^{-4} W kg^{-1}) [43,44].

IV. REMARKS

We have quantified Lagrangian statistics and pair dispersion induced by a single pulse of a small swimmer, and identified three stages dominated by flow acceleration, mixing, and dissipation based on the Lagrangian velocity statistics. With a careful characterization of the initial separation in the spatiotemporal domain, the pair dispersion indicates rich wake dynamics in each stage. Flow acceleration by the jellyfish propulsion induced bursts of $\sim t^3$ dispersion even at a low turbulence level due to large-scale inhomogeneity and unsteadiness of the flow, rather than the multiscale nature of strong turbulence in the Richardson-Obukhov regime. This is due to the unsteadiness in flow acceleration and two effective swimming mechanisms, namely, jetting and paddling. At the fully mixed stage, the dispersion exhibited $\sim t^2$ Batchelor scaling as a function of the initial separation similar to the case of homogeneous turbulence. An accurate estimation of Kolmogorov microscales generated by the jellyfish wake is computed and compared in Lagrangian and Eulerian frames of reference. The current work opens possibilities for further understanding of other swimming mechanisms such as turning [45] as well as predation [46], aggregation behavior [47], other small impulsive swimmers [48], migration strategy of phytoplankton in response to turbulent mixing [49], among others in a Lagrangian perspective.

ACKNOWLEDGMENTS

This work was supported by the Department of Mechanical Science and Engineering, University of Illinois, as part of the start-up package of L. P. Chamorro. The authors thank undergraduate student A. Uppal for the help during the experiments.

[1] A. La Porta, G. A. Voth, A. M. Crawford, J. Alexander, and E. Bodenschatz, Fluid particle accelerations in fully developed turbulence, Nature **409**, 1017 (2001).

[2] G. A. Voth, A. La Porta, A. M. Crawford, J. Alexander, and E. Bodenschatz, Measurement of particle accelerations in fully developed turbulence, J. Fluid. Mech. **469**, 121 (2002).

[3] N. Mordant, A. M. Crawford, and E. Bodenschatz, Experimental Lagrangian acceleration probability density function measurement, Physica D (Amsterdam) **193**, 245 (2004).

[4] L. Biferale, G. Boffetta, A. Celani, B. J. Devenish, A. Lanotte, and F. Toschi, Lagrangian statistics of particle pairs in homogeneous isotropic turbulence, Phys. Fluids **17**, 115101 (2005).

[5] L. F. Richardson, Atmospheric diffusion shown on a distance-neighbour graph, Proc. R. Soc. London A **110**, 709 (1926).

[6] A. M. Obukhov, Spectral energy distribution in a turbulent flow, Izv. Akad. Nauk SSSR **5**, 453 (1941).

[7] G. K. Batchelor, The application of the similarity theory of turbulence to atmospheric diffusion, Q. J. R. Meteorol. Soc. **76**, 133 (1950).

[8] M. Bourgoin, N. T. Ouellette, H. Xu, J. Berg, and E. Bodenschatz, The role of pair dispersion in turbulent flow, Science **311**, 835 (2006).

[9] J. P. Salazar and L. R. Collins, Two-particle dispersion in isotropic turbulent flows, Annu. Rev. Fluid Mech. **41**, 405 (2009).
[10] B. L. Sawford, P. K. Yeung, and J. F. Hackl, Reynolds number dependence of relative dispersion statistics in isotropic turbulence, Phys. Fluids **20**, 065111 (2008).
[11] N. T. Ouellette, H. Xu, and E. Bodenschatz, A quantitative study of three-dimensional Lagrangian particle tracking algorithms, Exp. Fluids **40**, 301 (2006).
[12] T. Ishihara and Y. Kaneda, Relative diffusion of a pair of fluid particles in the inertial subrange of turbulence, Phys. Fluids **14**, L69 (2002).
[13] P. K. Yeung, S. B. Pope, and B. L. Sawford, Reynolds number dependence of Lagrangian statistics in large numerical simulations of isotropic turbulence, J. Turbul. **7**, N58 (2006).
[14] R. Ni and K.-Q. Xia, Experimental investigation of pair dispersion with small initial separation in convective turbulent flows, Phys. Rev. E **87**, 063006 (2013).
[15] J.-T. Kim, S. Shen, S. L. DiMarco, Y. Jin, and L. P. Chamorro, On the Lagrangian acceleration in Rayleigh-Bénard convection at various aspect ratios, Phys. Rev. Fluids **3**, 113502 (2018).
[16] J. H. LaCasce and C. Ohlmann, Relative dispersion at the surface of the Gulf of Mexico, J. Mar. Res. **61**, 285 (2003).
[17] J. I. Polanco, I. Vinkovic, N. Stelzenmuller, N. Mordant, and M. Bourgoin, Relative dispersion of particle pairs in turbulent channel flow, Int. J. Heat Fluid Fl. **71**, 231 (2018).
[18] F. Toschi and E. Bodenschatz, Lagrangian properties of particles in turbulence, Annu. Rev. Fluid Mech. **41**, 375 (2009).
[19] F. Toschi, L. Biferale, G. Boffetta, A. Celani, B. J. Devenish, and A. Lanotte, Acceleration and vortex filaments in turbulence, J. Turbul. **6**, N15 (2005).
[20] J. Schumacher, Lagrangian Dispersion and Heat Transport in Convective Turbulence, Phys. Rev. Lett. **100**, 134502 (2008).
[21] R. Ni, S.-D. Huang, and K.-Q. Xia, Lagrangian acceleration measurements in convective thermal turbulence, J. Fluid Mech. **692**, 395 (2012).
[22] J.-T. Kim, Z. Zhang, A. Liberzon, Y. Zhang, and L. P. Chamorro, On the Lagrangian features of circular and semicircular jets via 3D particle tracking velocimetry, Exp. Therm. Fluid Sc. **77**, 306 (2016).
[23] N. Stelzenmuller, J. I. Polanco, L. Vignal, I. Vinkovic, and N. Mordant, Lagrangian acceleration statistics in a turbulent channel flow, Phys. Rev. Fluids **2**, 054602 (2017).
[24] M. Holzner, V. L. Morales, M. Willmann, and M. Dentz, Intermittent Lagrangian velocities and accelerations in three-dimensional porous medium flow, Phys. Rev. E **92**, 013015 (2015).
[25] S. P. Colin and J. H. Costello, Morphology, swimming performance and propulsive mode of six co-occurring hydromedusae, J. Exp. Biol. **205**, 427 (2002).
[26] J. O. Dabiri, S. Colin, and J. Costello, Morphological diversity of medusan lineages constrained by animal-fluid interactions, J. Exp. Biol. **210**, 1868 (2007).
[27] J. C. Nawroth, H. Lee, A. W. Feinberg, C. M. Ripplinger, M. L. McCain, A. Grosberg, J. O. Dabiri, and K. K. Parker, A tissue-engineered jellyfish with biomimetic propulsion, Nat. Biotechnol. **30**, 792 (2012).
[28] M. McHenry, Comparative biomechanics: The jellyfish paradox resolved, Curr. Biol. **17**, R632 (2007).
[29] M. Sahin and K. Mohseni, An arbitrary Lagrangian-Eulerian formulation for the numerical simulation of flow patterns generated by the hydromedusa *Aequorea victoria*, J. Comput. Phys. **228**, 4588 (2009).
[30] B. J. Gemmell, J. H. Costello, S. P. Colin, C. J. Stewart, J. O. Dabiri, D. Tafti, and S. Priya, Passive energy recapture in jellyfish contributes to propulsive advantage over other metazoans, Proc. Natl. Acad. Sci. USA **110**, 17904 (2013).
[31] B. J. Gemmell, J. Costello, and S. Colin, Exploring vortex enhancement and manipulation mechanisms in jellyfish that contributes to energetically efficient propulsion, Commun. Integr. Biol. **7**, e29014 (2014).
[32] T. P. Chang, N. A. Wilcox, and G. B. Tatterson, Application of image processing to the analysis of three-dimensional flow fields, Opt. Eng. **23**, 283 (1984).
[33] R. Racca and J. Dewey, A method for automatic particle tracking in a three-dimensional flow field, Exp. Fluids **6**, 25 (1988).
[34] N. A. Malik, T. Dracos, and D. A. Papantoniou, Particle tracking velocimetry in three-dimensional flows, Exp. Fluids **15**, 279 (1993).

[35] M. Kreizer and A. Liberzon, Real-time image processing for particle tracking velocimetry, Exp. Fluids **48**, 105 (2010).
[36] J. O. Dabiri, S. P. Colin, J. H. Costello, and M. Gharib, Flow patterns generated by oblate medusan jellyfish: Field measurements and laboratory analyses, J. Exp. Biol. **208**, 1257 (2005).
[37] P. Craven and G. Wahba, Smoothing noisy data with spline functions, Numer. Math. **31**, 377 (1978).
[38] M. A. T. van Hinsberg, J. H. M. Boonkkamp, F. Toschi, and H. J. H. Clercx, Optimal interpolation schemes for particle tracking in turbulence, Phys. Rev. E **87**, 043307 (2013).
[39] J.-T. Kim, D. Kim, A. Liberzon, and L. P. Chamorro, Three-dimensional particle tracking velocimetry for turbulence applications: Case of a jet flow, JoVE **108**, e53745 (2016).
[40] B. J. Gemmell, D. R. Troolin, J. H. Costello, S. P. Colin, and R. A. Satterlie, Control of vortex rings for manoeuvrability, J. R. Soc. Interface **12**, 108 (2015).
[41] W. Heisenberg, Zur statistichen theorie der turbulenz, Z. Phys. **124**, 628 (1948).
[42] A. M. Yaglom, On the acceleration field in a turbulent flow, C. R. Akad. USSR **67**, 795 (1949).
[43] E. Kunze, J. F. Dower, I. Beveridge, R. Dewey, and K. P. Bartlett, Observations of biologically generated turbulence in a coastal inlet, Science **313**, 1768 (2006).
[44] K. Katija and J. O. Dabiri, A viscosity-enhanced mechanism for biogenic ocean mixing, Nature **460**, 624 (2009).
[45] R. A. Satterlie, Neuronal control of swimming in jellyfish: A comparative story, Can. J. Zool. **80**, 1654 (2002).
[46] J. Shoji, R. Masuda, Y. Yamashita, and M. Tanaka, Predation on fish larvae by moon jellyfish *Aurelia aurita* under low dissolved oxygen concentrations, Fisheries Sci. **71**, 748 (2005).
[47] J. E. Purcell, E. D. Brown, K. D. E. Stokesbury, L. H. Haldorson, and T. C. Shirley, Aggregations of the jellyfish *Aurelia labiata*: Abundance, distribution, association with age-0 walleye pollock, and behaviors promoting aggregation in Prince William Sound, Alaska, USA, Mar. Ecol. Prog. Ser. **195**, 145 (2000).
[48] I. A. Houghton, J. R. Koseff, S. G. Monismith, and J. O. Dabiri, Vertically migrating swimmers generate aggregation-scale eddies in a stratified column, Nature **556**, 497 (2018).
[49] A. Sengupta, F. Carrara, and R. Stocker, Phytoplankton can actively diversify their migration strategy in response to turbulent cues, Nature **543**, 555 (2017).